Assessment of Corrosion and Scratch Resistance of Plasma Electrolytic Oxidation and Hard Anodized Coatings Fabricated on AA7075-T6

Article *in* Transactions of the Indian Institute of Metals · May 2021

DOI: 10.1007/s12666-021-02289-4

CITATIONS
8

READS
72

8 authors, including:

Premchand Chennampalli
National Institute of Technology Tiruchirappalli
11 PUBLICATIONS **61** CITATIONS
SEE PROFILE

Sai Kiran Amruthaluru
Indian Maritime University
24 PUBLICATIONS **201** CITATIONS
SEE PROFILE

Manojkumar Palanivel
National Institute of Technology Tiruchirappalli
19 PUBLICATIONS **92** CITATIONS
SEE PROFILE

N. Rameshbabu
National Institute of Technology Tiruchirappalli, India
81 PUBLICATIONS **2,541** CITATIONS
SEE PROFILE

Trans Indian Inst Met (2021) 74(8):1991–2002
https://doi.org/10.1007/s12666-021-02289-4

ORIGINAL ARTICLE

Assessment of Corrosion and Scratch Resistance of Plasma Electrolytic Oxidation and Hard Anodized Coatings Fabricated on AA7075-T6

C. Premchand[1] · S. Hariprasad[1] · A. Saikiran[1] · E. Lokeshkumar[1] · P. Manojkumar[1] · B. Ravisankar[1] · B. Venkataraman[2] · N. Rameshbabu[1]

Received: 20 March 2021 / Accepted: 30 April 2021 / Published online: 31 May 2021

Abstract Surface modification of high-strength aluminium alloy 7075-T6 by plasma electrolytic oxidation (PEO) and type II hard anodization (HA) is presented in the current work. PEO-based ceramic oxide coatings were fabricated by employing an alternating current (AC) power source with a current density of 300 mA/cm^2. The concentration effect of electrolytes on the alumina coatings was investigated and optimized comprehensively. Three separate aqueous electrolytes with 1:3, 1:1 and 3:1 proportions of sodium silicate (Na_2SiO_3) and potassium hydroxide (KOH) were utilized to evaluate optimum electrolyte concentration for obtaining desired AC-PEO coatings. X-ray diffraction (XRD) was utilized to investigate the phase composition of the coatings. Field emission scanning electron microscopy (FESEM) was employed to investigate the surface and cross-sectional characteristics of oxide coatings. Scratch testing was used to assess the oxide coatings' adhesion ability, and potentiodynamic polarization (PDP) was utilized to assess the coatings' corrosion behaviour in a 3.5 wt% aqueous NaCl solution. Among the AC-PEO and HA coatings, the AC-PEO specimen fabricated with equal ratios of sodium silicate and KOH concentration (Na_2SiO_3:KOH 1:1) showed excellent adhesion strength (critical load, L_c = 41.5 N) along with the remarkable corrosion resistance (corrosion current density, $i_{corr} = 5.63 \times 10^{-6}$ mA/cm^2).

✉ N. Rameshbabu
nrb@nitt.edu

[1] Department of Metallurgical and Materials Engineering, National Institute of Technology, Tiruchirappalli 620015, India

[2] Defence Metallurgical Research Laboratory, P.O. Kanchanbagh, Hyderabad 500048, India

Keywords AA7075-T6 · Adhesion strength · Corrosion resistance · Electrolyte composition · PEO · Type II hard anodization

1 Introduction

Aluminium and its alloys have an extensive scope of utility in the aerospace industry, automotive, commercial and military fighter aircraft manufacturing due to its magnificent features such as maximum strength-to-weight ratio, formability and lightweight [1–4]. The defence combat aircrafts are served in coastal zones and they are exposed to the Cl^- ions existing in the atmosphere, which can destroy the native oxide film on AA7075. The formation of Mg(Zn, Cu, Al)$_2$ precipitates anodic to the aluminium matrix results in the higher corrosive behaviour of aluminium alloy [5]. Thus, suitable surface alteration technique is required to get the desired protection against corrosion. Nowadays, various surface modification techniques such as anodizing [6–8], CVD [9], sol–gel [10], PVD [11], cold spraying [12], plasma spraying [13], laser deposition [14], electrodeposition and electrophoretic deposition (EPD) [15–17] are used. Most of these conventional processes involve peak temperatures, which further needs great control and care over the process [18]. Hard anodizing (HA) is a good surface treatment process for high-strength aluminium alloys to improve tribological properties.

Among the different variants of aluminium anodizing, sulphuric acid-based anodizing shows improved corrosion and wear properties and is commonly used in marine and aerospace applications [19]. Hard anodizing provides a wide range of industrial applications with characteristics that make aluminium alloys more competitive than steel.

The wear characteristics of hard anodized aluminium alloys may be greater than and equal to the hardened steel case, providing aluminium alloy parts for use in applications where only hardened steel was formerly used [20]. Plasma electrolytic oxidation (PEO) is a burgeoning novel surface conversion technique used to develop thicker and adherent ceramic oxide coatings with the help of electrolytic plasma discharges mainly on valve metals, i.e. zirconium, aluminium, magnesium, titanium, niobium, and their alloys [20–29]. Out of the various surface conversion processes, the PEO is the electrolytic process and has benefits of being economical and simple. At the same time, it is so efficient due to the generation of a denser oxide coating with better adhesion, wear resistance and corrosion resistance. In conventional hard anodizing (HA), the oxide film is established due to ionic diffusion through the oxide coating without considerable effect on the substrate [30] and the process is executed in the range of 10–80 V. However, in PEO process, voltages reach beyond the breakdown potential of the oxide coatings, normally 200–800 V. At these peak voltages, a spark is produced due to local dielectric breakdown of oxide coating and rapidly gets discharged in electrolyte within no time [31]. PEO coating properties mainly depend on the process variables, namely electrolyte composition, electrical process variables (current density, breakdown voltage, frequency, and duty cycle) and oxidation time [32–34]. PEO coating developed in DC mode provides minimal oxide growth rate, high porosity, and limited control on plasma discharges than AC mode. AC mode of PEO coatings has attracted the researcher's attention due to improved coating properties compared to DC mode [35]. DC PEO has published a substantial amount of research on the production of oxide coatings on Al alloys, but only a meagre amount of work is proclaimed on alternative current (AC) mode PEO coatings and its comparison with the hard anodized (HA) coatings.

Arunnellaiappan et al. fabricated ceramic coatings on AA7075 by PEO route with varying frequency and duty cycle using a DC power source. They observed that the duty cycle and frequency have a significant effect on the surface features, coating formation, coating thickness, scratch resistance and corrosion behaviour of the DC PEO coatings [5]. Yerokhin et al. developed ceramic coatings on Al alloys by PEO. They observed the effect of pulse current on the kinetics of coating build-up and energy efficiency of the process [36]. Ghafaripoor et al. produced composite coatings on AA 7075 in sodium metasilicate (Na_2SiO_3)-based electrolyte containing 200 nm diameter α-alumina particles. They observed that the variation in the concentration of α-Al_2O_3 nanoparticles showed a detrimental effect on the coating's tribo-corrosion characteristics [37]. Kwolek et al. fabricated oxide coatings on 6061-T6 aluminium alloy by hard anodizing and noticed that the abrasion and scratch resistance of the oxide layers enhanced with increased thickness [38]. Ramakrishna et al. correlated the tribological behaviour of hard anodizing films with the micro-arc oxidation (MAO) coatings developed on AA6061-T6. The MAO coatings and hard anodized coatings displayed superior tribological behaviour compared to AA6061. They recognized that HA coatings exhibited poor wear resistance with a 6–15 times higher wear rate compared to MAO coatings. Under erosion conditions, HA coatings exhibited tenfold higher erosion rate than MAO coatings [39]. Becerik et al. analysed the effect of sodium metasilicate concentration (7.5 g/l Na_2SiO_3 and 15 g/l Na_2SiO_3) on several surface features and corrosion behaviour of 6060 Al alloy, and they proclaimed that the coating prevailed in an electrolyte comprising of 15 g/l Na_2SiO_3 exhibiting low surface roughness, enhanced hardness and corrosion resistance [40]. Fattah-Alhosseini et al. analysed the effect of various concentrations of Na_2SiO_3 and KOH on surface morphology, chemical composition, and electrochemical behaviour of PEO oxide coatings on the AA6061. They concluded that the higher concentrations of sodium metasilicate (4 g/l) resulted in the surge of Si embodiment in the coating, thereby resulting in an increase in coating thickness and corrosion resistance [41]. Sharma et al. studied the effect of KOH:Na_2SiO_3 ratio (5:5, 5:10, 10:5, 10:10, 15:5, and 15:10) on hardness and microstructure of PEO oxide coatings on AA6061. They reported that the coating exhibited peak hardness and favourable microstructural features at KOH:Na_2SiO_3 ratio of 15:10 followed by 10:10 [18]. To the best of the authors' awareness, no work is found on optimizing the electrolyte concentration to enhance the surface morphology, indentation scratch resistance and corrosion resistance of the AC-PEO coatings on the high-strength aluminium alloys in contrast to the hard anodized coatings. The present study aspires to explain the effect of electrolyte concentration on the coatings' surface morphology, thickness, corrosion resistance, and the scratch resistance of the AC-PEO-treated 7075-T6 Al alloy compared to type II hard anodized coatings. The phases present in the oxide coatings were examined by the XRD. The elemental composition of coatings, cross section and surface morphological features were analysed by the FESEM equipped with an energy-dispersive spectroscopy (EDS). The coating thickness, surface features, corrosion, and scratch resistance of the AC-PEO coatings were correlated with type II hard anodized coatings and aluminium substrate.

2 Materials and Analysing Methods

2.1 Preparation of Samples

In this study, aluminium alloy 7075 -T6 in heat-treated condition with a nominal composition of 6.11% Zn, 2.53% Mg, 1.42% Cu, 0.28% Cr, 0.49% Fe, 0.17% Ti, 0.38% Si, 0.24% Mn and surplus aluminium was used as substrate. Rectangular coupons with 20 mm × 18 mm × 3 mm dimensions were adopted as substrate materials, and those were polished mechanically with various grades of silicon carbide emery paper (400, 800, 1000 and 1200 grit). The polished specimens were cleaned with acetone for 15 s, ultrasonically cleaned in deionized water for 5 min, hot air-dried and stored in an airtight desiccator. Around 50 coupons were kept ready for subsequent coatings preparation and its characterization.

2.2 Fabrication of PEO Coatings

An alternating current (AC) power source with a 1000 V maximum potential and a 20 A maximum current was adopted for the development of coatings. Prior to the PEO coating process, to remove contamination on a sample surface, the specimens were immersed in an acid pickling bath containing aqueous nitric acid (300 g/l) for 3 min followed by the alkaline degreasing with commercial cleaner (5 wt% Turco 4215 NC-LT in deionized water) to remove acidic remnants and rinsed with distilled water. PEO coatings were fabricated by measuring a current density of 300 mA/cm^2 throughout the process duration of 30 min. Three different compositions of electrolytes containing different amounts of potassium hydroxide (KOH) and sodium silicate (Na_2SiO_3) were used for fabricating the PEO coatings and are presented in Table 1. The electrolyte bath comprising of different proportions of Na_2SiO_3 and KOH was kept at a steady temperature of 20 °C throughout the PEO process with the help of chiller to overcome the thermal effects on the growth of the AC-PEO coatings. At the coating fabrication time, the electrolyte solution is continuously agitated by an external magnetic stirrer to maintain the compositional homogeneity throughout the process. The identification names of samples AC-PEO processed with different electrolyte compositions, i.e. KOH rich (1:3 ratio of Na_2SiO_3 and KOH), equal-proportioned (1:1 ratio of Na_2SiO_3 and KOH) and sodium metasilicate rich (3:1 ratio of Na_2SiO_3 and KOH) are listed in Table 1. Hereafter, uncoated substrate and AC-PEO fabricated samples will be referred with identification codes as S, A, B and C, respectively, in the manuscript.

Table 1 The sample codes used for AC-PEO coatings with their corresponding electrolyte composition, and electrical conductivity

PEO sample code	Electrolyte composition (g/L)	Conductivity (mS/cm)
A	2.5 Na_2SiO_3 + 7.5 KOH	28.3
B	5 Na_2SiO_3 + 5 KOH	13.2
C	7.5 Na_2SiO_3 + 2.5 KOH	15.3

Table 2 Experimental conditions for developing PEO and HA coatings

Parameters	Plasma electrolytic oxidation	Hard anodizing
Electrolyte bath	Na_2SiO_3 and KOH (2.5–7.5 g/L)	H_2SO_4 (2 M)
Power source	AC	DC
Bath temperature	20 °C	5 °C
Current density (A/cm^2)	0.3	0.03

2.3 Fabrication of Hard Anodized (HA) Coatings

Type II hard anodized (HA) coatings were fabricated on aluminium alloy 7075-T6 samples. Foregoing to the HA coating process, to remove contamination on a sample surface, the specimens were cleaned following the same procedure adopted before the PEO coatings, as described in Sect. 2.2. After cleaning process, the samples were loaded in the H_2SO_4 electrolyte bath to produce hard anodized coatings. The process parameters utilized for HA coatings along with PEO coatings are recorded in Table 2.

2.4 Characterization of PEO and HA Coatings

The phase identification of the oxide-coated specimens was performed through the X-ray diffractometer (Rigaku Ultima IV, Japan), equipped with an energy source operated at 30 mA and 40 kV, using a copper target emitting K_α radiation (λ = 1.5406 Å) operating over a selected scanning span of 20°–90° at a speed of 0.016°/s with an interval of 0.05°. Phases of the coatings were identified by using the standard JCPDS data cards. The morphological features along with the elemental analysis over the surface of the coatings were assessed by a FESEM (field emission scanning electron microscope, GEMINI-300, Carl Zeiss, Germany) attached with the energy-dispersive X-ray spectrometer (EDS). The voltages 4 kV and 20 kV were used for FESEM imaging and EDS elemental composition analysis of the coated samples. The HA and PEO coated sample's average thickness was assessed from the cross-sectional FESEM micrographs taken over eight distinct locations for every individual sample. The coating

thickness was also evaluated using eddy current-based digital thickness apparatus (Qnix premium-8500, Germany) with a precision of ± 0.05 µm. Surface three-dimensional (3D) morphology and depth profiles of the fabricated oxide coatings were evaluated with lateral and vertical resolutions in the order of 0.3 µm and 0.1 nm, using white light interferometer (Taylor Hobson Talysurf CCI). Surface roughness values were calculated by performing line scans over a length of 0.8 mm at ten different locations on two replicates for each sample, and the average values are reported. Surface roughness measurements were evaluated at a magnification of 200× using the objective lens of 20×. The bonding strength between oxide coating and substrate was investigated as per ASTM standard C1624-05 with the aid of an automatic indentation scratch testing unit (CSM Revetest, Switzerland) rigged with a spheroidal diamond probe with a 200 µm tip radius. Scratch test was carried out under progressive loading conditions ranging from 1 to 50 N (24.5 N/min) with an indenter advancing rate of 2.5 mm/min over a track length of 5 mm.

Corrosion properties of bare and PEO-coated AA7075-T6 specimens were estimated by potentiodynamic polarization test (PDP), adopting a computerized potentiostat (Gill AC, ACM instruments, Cumbria, UK). PDP test was carried out on the samples (working electrode) by covering an area of 0.5 cm^2 to a 3.5 wt% NaCl corrosive medium by polarizing the samples over a potential range of − 500 to 3000 mV around the open circuit potential (OCP) at a rate of 0.166 mV/s (ASTM G 59-97) against a platinum foil (auxiliary electrode). The PDP measurements were validated at least three times to ensure reproducibility. The potential values were determined by using a reference electrode, saturated calomel electrode (SCE). The corrosion voltage and current of the samples were assessed by employing the Tafel extrapolation method over the linear portion of the cathodic and anodic curves (± 250 mV) around open circuit potential (OCP).

3 Results and Discussion

3.1 Voltage–Time (V–t) Characteristics of AC-PEO Coatings

In the course of AC-PEO process, the variation of voltage with process time was captured, and voltage–time (*V–t*) response of AA7075-T6 over a processing duration of 30 min is represented in Fig. 1. Hereafter, voltages were referred to the root-mean-square (rms) voltages in the manuscript. The coating growth mechanism of the PEO process can be elaborated by *V–t* curves, and it is mainly categorized into three states such as anodization, unstable PEO and stable PEO regions [18]. In the beginning, voltage increases linearly with processing time. It is mainly because of developing a nonconducting oxide film at the juncture of the substrate and electrolyte via traditional anodizing. Further, the voltage reaches the breakdown voltage (V_b), and several microsparks are sighted on sample surface illustrating the initiation of PEO process, during which a relatively sluggish escalation in the voltage is observed compared to the anodization attributing to the small and dense microsparks affiliated with electronic current. In the final state, a considerable increase in voltage can be observed with time. The breakdown and final voltages of AC-PEO coatings are presented in Table 3.

The breakdown voltage (V_b) is related to the conductivity of electrolyte conferring to the following relation $V_b = a_B + b_B\ (k^{-1})$ [42, 43], where a_B and b_B are constants related to substrate and electrolyte having a conductivity *k*. The breakdown voltages for specimens A, B and C are 162, 201 and 184 V, respectively. The observed breakdown voltages (V_b) in this study are lower than those observed in the typical PEO coatings developed using a DC source [44]. Specimen B exhibits the highest breakdown voltage due to low electrolyte conductivity, and specimen A displays the lowest breakdown voltage, due to high conductivity and higher KOH concentration of electrolyte. The higher concentration of KOH in the electrolyte may dissolve the formed oxide films during anodization stage [45].

3.2 Phase Identification of the Coatings

X-ray diffraction patterns of the uncoated substrate (S), AC-PEO-treated samples A, B, C and HA sample are presented in Fig. 2. The XRD pattern of the bare substrate

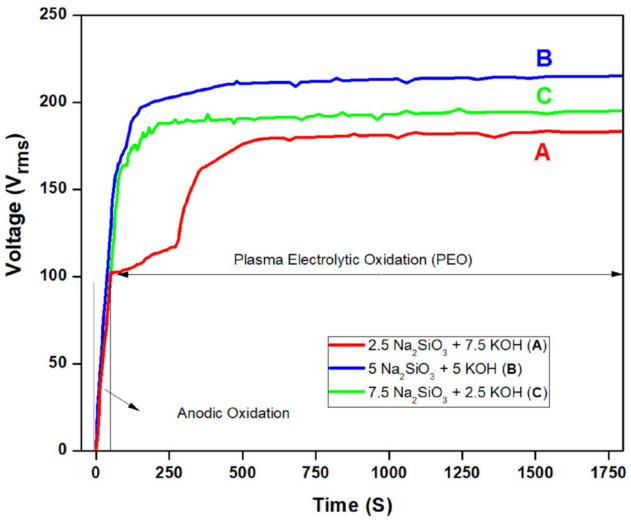

Fig. 1 Voltage–time characteristics of the PEO-treated samples A, B, C

Table 3 Electrolyte conductivity and breakdown voltages of AC-PEO coatings

PEO sample code	Conductivity (mS/cm)	Breakdown voltage, V_{rms} (± 2 V)
A	28.3	162
B	13.2	201
C	15.3	184

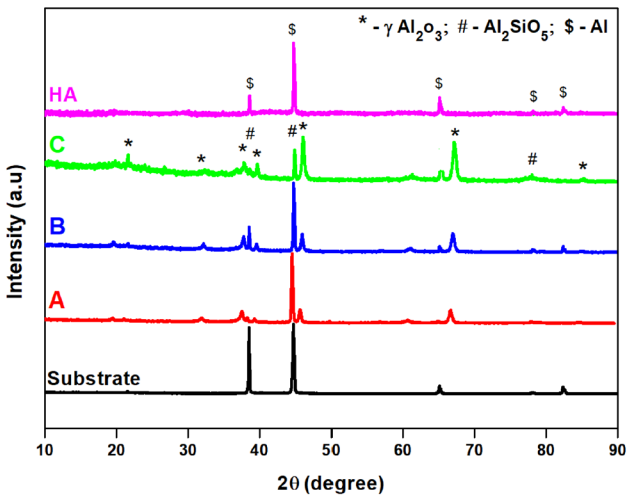

Fig. 2 XRD patterns of the substrate (S), PEO-treated samples A, B, C and HA sample

reveals Al peaks (JCPDS No. 894037) alone. PEO-coated samples display the peaks of γ-Al_2O_3 (JCPDS No. 100425) which implies that the coatings are chiefly consisting of γ-Al_2O_3 phase along with the substrate Al peaks. Similar diffraction patterns are noticed in all PEO samples, namely A, B and C, which mainly contain γ-Al_2O_3 along with Al_2SiO_5 (JCPDS No. 83-1567) peaks. Al_2SiO_5 phase is formed mainly due to the reaction of SiO_3^{2-} ions from the sodium metasilicate electrolyte and Al^{3+} ions from the aluminium substrate. On the other side, only substrate Al peaks are shown in the HA sample, which might be due to the amorphous oxide layer developed during the process.

3.3 Surface Morphology and EDS Spectra of the Oxide Coatings

The FESEM surface morphology of the AC-PEO coatings A, B, C, and hard anodized sample HA is presented in Fig. 3. Different electrolyte compositions adopted in the PEO treatment firmly affects the discharge characteristics of the oxide coatings, thereby resulting in different surface morphologies observed in PEO samples A, B and C. PEO-treated samples show pores, because of gas evolution and metal-oxide ejection through the microdischarge channels developed in the interim of PEO process. Microcracks on PEO-coated surfaces are due to thermal shocks associated with the fused metal oxide's sudden cooling. Samples B and C evince pancake structures, due to the cool-down of the ejected molten oxide through microdischarge channels during oxide film formation. Due to the initial delay in the PEO phase, specimen A does not show a similar structure, which is mainly because of the disintegration of coatings during the initial stage, and this is attributed to the maximum concentration of KOH. The average surface porosity and the average pore size of the coatings were measured by the ImageJ software. The average surface porosity is calculated by the relative area of the surface covered by the pores. The percentage surface porosity values of the samples A, B, C and HA are around 2.54, 1.42, 2.27 and 1.03, respectively. The average pore size values of the samples A, B, C and HA are 0.6 ± 0.1 µm, 1.7 ± 0.2 µm, 0.8 ± 0.2 µm and 1.5 ± 0.1 µm, respectively. Sample A shows a large number of surface pores in contrast to samples B and C; the pore size is noted to be tiny. The variation in the concentration of KOH and silicate has a significant effect on the coatings' surface morphology. On the other hand, the HA sample shows few microcracks throughout the entire coating, for the weaker junctions along the oxide cell's boundaries. In the case of PEO samples, due to the aggressive coating formation around the discharge channels, the coatings' surface is uneven, but the coatings show high bonding strength between the substrate and form oxide film. While the HA coating is even and have smooth surface features. The surface EDS spectra outcomes of the AC-PEO-treated and HA coatings are presented in Fig. 4. These findings imply that the oxide coatings display the characteristic peaks related to Al, O, Mg and Zn. In supplement to that, PEO samples show Si (silicon) and K (potassium) elements and HA sample shows sulphur (S) element. The maximum intensity peaks related to the aluminium (Al) and oxygen (O) show that the alumina (Al_2O_3) is the predominant phase in the coatings, which is endorsed by the higher Al and O content, as shown in Table 4. It is mainly due to low silicate content and onset delay during the AC-PEO process. But the HA sample shows sulphur (S) element due to H_2SO_4 solution used for treatment.

3.4 Profilometric Studies of the Coatings

The average surface roughness (R_a) values of the oxide coatings are presented in Table 5. The roughness values of the coatings A, B, C and HA are 3.2 ± 0.2 µm, 4.1 ± 0.3 µm, 4.9 ± 0.3 µm, and 1.4 ± 0.1 µm, respectively. Among the three AC-PEO coatings, sample A exhibits fewer hills and valleys than sample B and C, which can be ascribed to the hamper in the inception of the

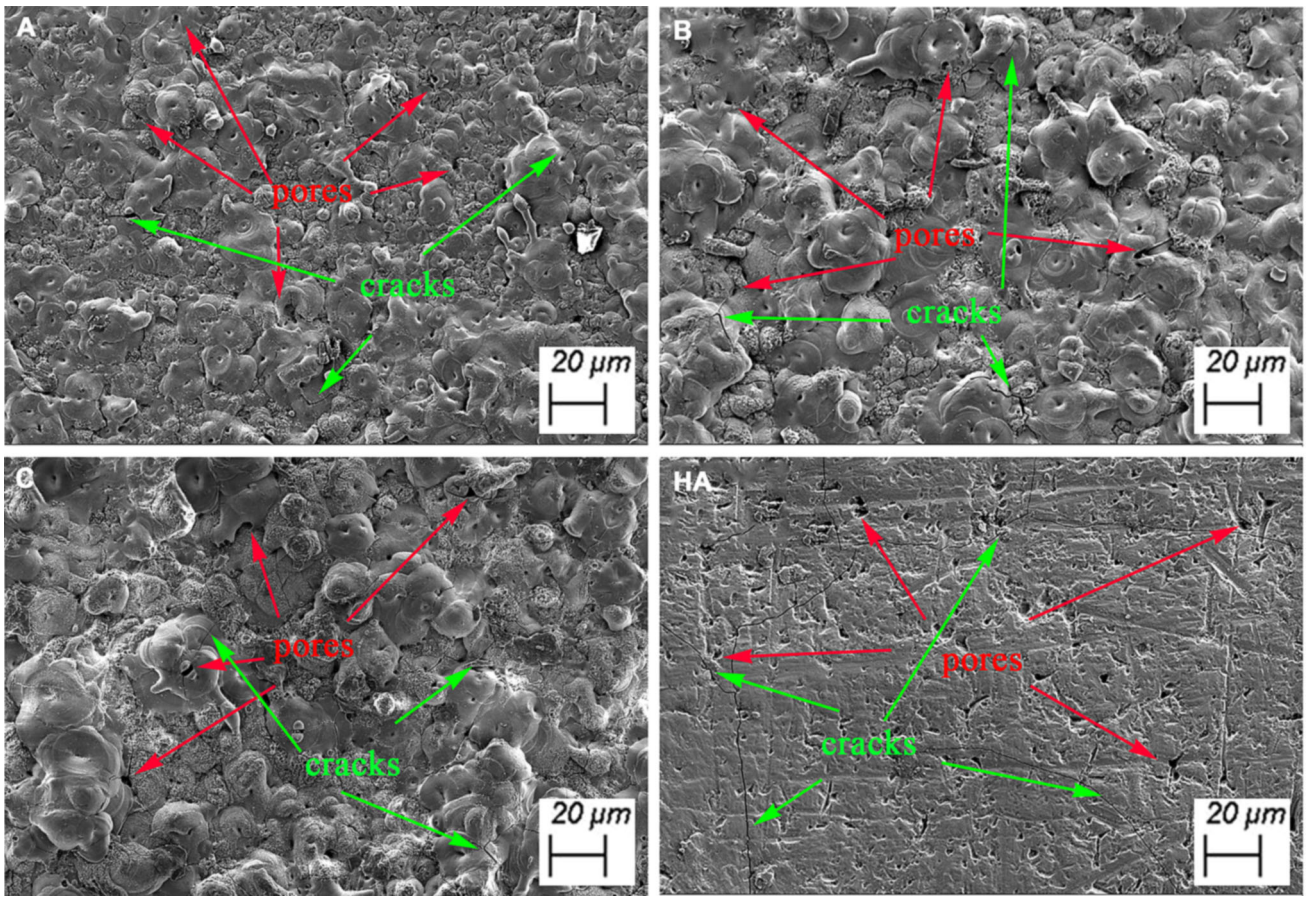

Fig. 3 FESEM surface morphology of the PEO-treated samples A, B, C and HA sample

coating during the PEO coating process. The surface roughness relies on the differences in pore morphology, structure of oxide coatings and microcracks. Figure 5 presents the 3D surface profile and depth profile of the formulated coatings. The three-dimensional optical profiles of the PEO coating surfaces disclose more significant number of valleys and hills. In contrast to PEO treated samples, the HA sample exhibits a much smaller number of valleys and hills. The depth profiles also corroborate that the HA sample shows shallow valleys contrast to AC-PEO coatings (A, B and C), as endorsed by the FESEM surface micrographs portrayed in Fig. 3.

3.5 Thickness of the Oxide Coatings

The cross-sectional morphologies of the oxide coatings are presented in Fig. 6. The thickness of the coatings evaluated by the eddy current thickness gauge agrees with the thickness evident from the FESEM cross-sectional micrographs shown in Fig. 6. PEO coatings contain two layers, i.e. outer porous and inner barrier layers, as indicated by the green and red line boundaries, respectively, whereas HA coatings exhibit single-layered structure as shown in Fig. 6. The average thickness values of the coated specimens are found to be 40 ± 1 μm, 43 ± 1.3 μm, 46 ± 0.5 μm and 44 ± 1.2 μm for A, B, C and HA samples, respectively. Sample A shows the least thickness due to the delay in the onset of the microdischarges. This is because of the dissolution action of the developed oxide coating by higher KOH concentration in the electrolyte [46]. The growth rate for the oxide coating is known to be nearly in proportion to liberated microdischarges, by means of which fused metal oxide is expelled and forms a surface coating. In general, there are two apparent layers in the PEO coatings, a dense inner layer and a loose porous outer layer as depicted in Fig. 6.

3.6 Adhesion Strength of the Coatings

The adhesion strength of the developed oxide coatings was examined by using a single-point scratch testing equipment. Figure 7 shows the applied load versus friction force curves along with the optical microscopic scratch track images of the HA sample and PEO coatings A, B and C. Figure 8 also shows the corresponding FESEM images of the scratch tracks. During the scratch indentation test, the

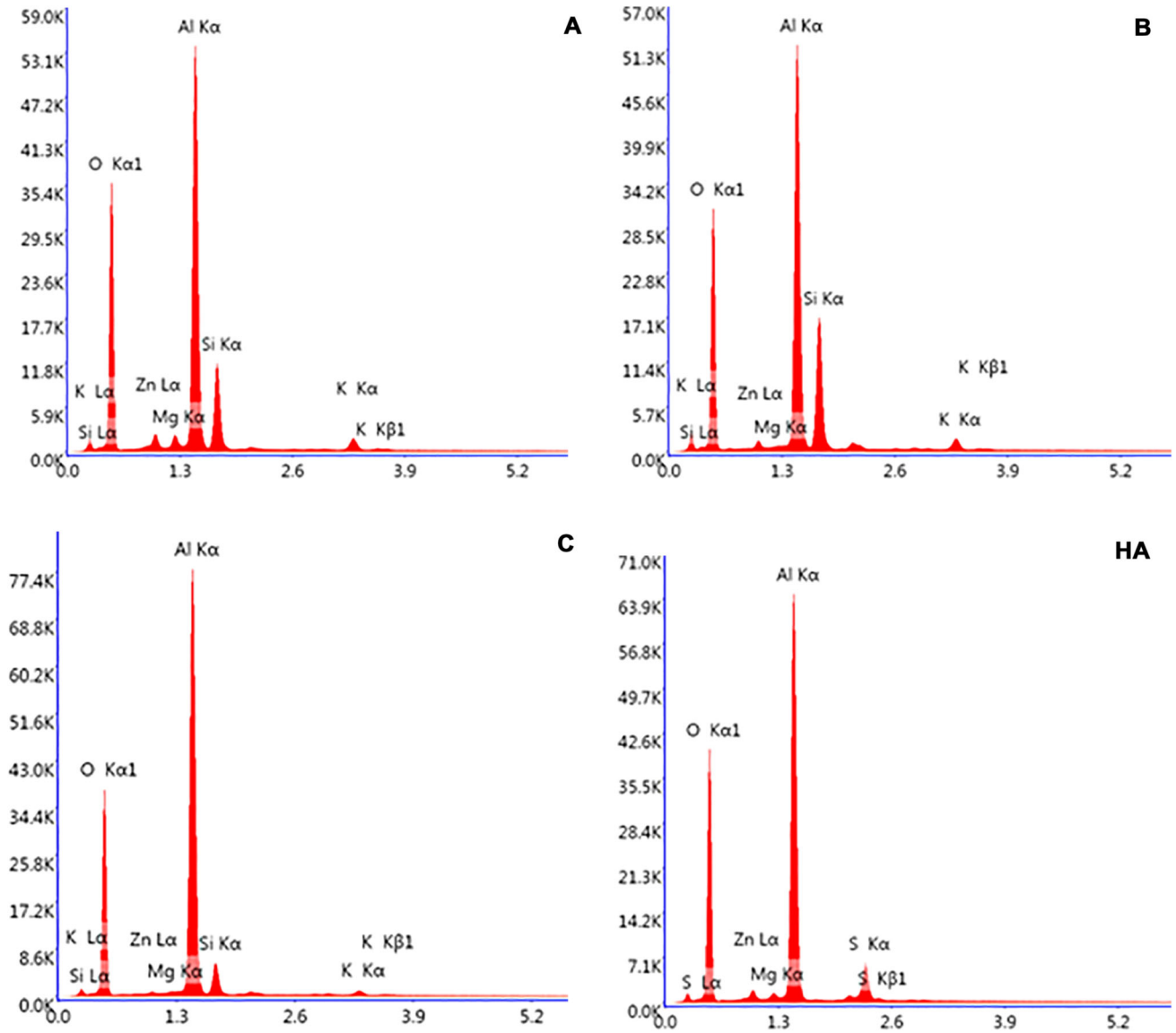

Fig. 4 EDS spectra of the PEO-treated samples A, B, C and HA sample

Table 4 Elemental composition of the PEO treated samples (A, B and C) and hard anodizing (HA) sample

Sample code	A	B	C	HA
Elements	(at.%)	(at.%)	(at.%)	(at.%)
O	57.38	61.14	58.03	61.14
Mg	0.35	0.32	0.22	0.79
Al	37.10	28.84	28.02	33.04
Si	4.27	8.23	12.31	–
K	0.56	1.14	1.11	–
Zn	0.34	0.33	0.31	0.67
S	–	–	–	4.36

load was increased progressively from 1 to 50 N, and the variations in the frictional force with the increasing applied load were studied. A visual examination of the scratch track can reveal the critical load at which a definitive failure of the coatings materializes. Frictional force according to the load at which delamination of the coating occurs is termed as critical load. The critical load (L_c) values for the coated samples which are an indicative of the scratch resistance of the coatings are presented in Table 6. The thickness, hardness, porosity, and phase composition of the coatings strongly influence their scratch resistance [46]. The critical loads of the samples A, B, C and HA are 33.5 (± 2.2) N, 41.5 (± 1.8) N, 37 (± 1.5) N and 28 (± 0.7) N, respectively. According to Amonton's first law, the friction force is proportional to the applied load through

Table 5 Coating thickness (t) and surface roughness (R_a) of the PEO-treated samples (A, B and C) and hard anodizing (HA) sample

Sample code	t (± 1 μm)	R_a (μm)
A	40	3.2 ± 0.2
B	43	4.1 ± 0.3
C	46	4.9 ± 0.3
HA	44	1.4 ± 0.1

the area of contact and corresponding friction forces of the samples A, B, C and HA are 9.4 (± 0.6) N, 13.1 (± 1.1) N, 11.8 (± 0.8) N and 5.7 (± 0.4) N, respectively. Adhesive failure of the coatings is apparent from the scratch tracks owing to the absence of the delamination adjacent to the tracks [47, 48]. The high scratch resistance of sample B can be referred to its higher resistance for Indentation. The PEO-coated sample C has high thickness than sample B, but sample C has lower critical load which may perhaps be

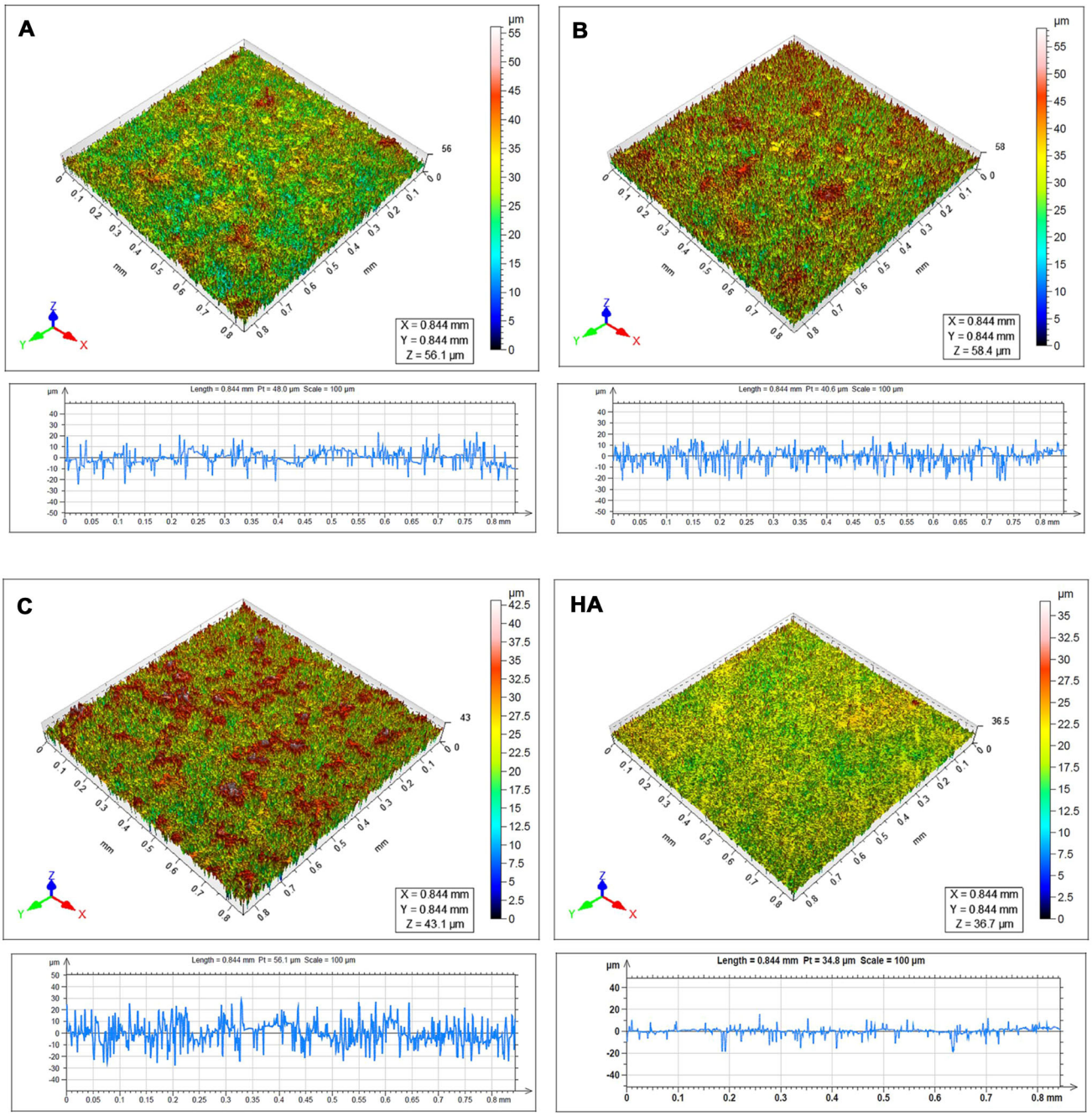

Fig. 5 3D surface profile and corresponding depth profile of the PEO-treated samples A, B, C and HA sample

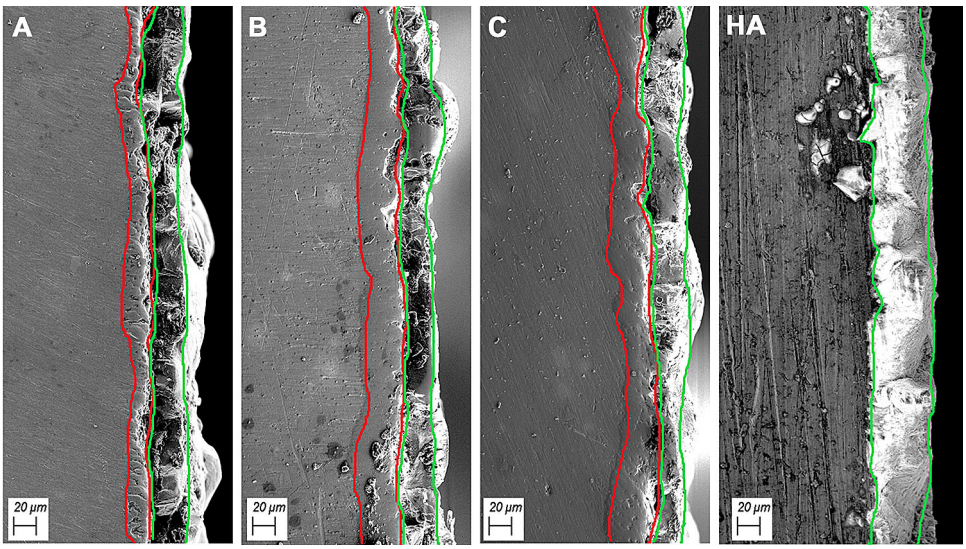

Fig. 6 FESEM cross-sectional micrographs of the PEO treated samples A, B, C and HA sample

ascribed to the existence of comparatively more pores and microcracks on the surface as observed from the surface FESEM images portrayed in Fig. 3. From Fig. 7, variation in the slope of frictional force vs. load curve and delamination of coating for the HA sample can be observed in the FESEM image. HA sample displays lower adhesion strength due to few microcracks throughout the coating and lower adhesion between the substrate and the coating interface. The HA sample shows lower critical load value (L_c = 28 (± 0.7) N) among all coatings. It is mainly because of the weak junctions along the oxide cell boundaries as clear from the surface FESEM microstructures illustrated in Fig. 3. Scratch resistance offered by PEO coatings (A, B and C) is superior to hard anodized (HA) coating.

3.7 Potentiodynamic Polarization (PDP) Studies

The corrosive behaviour of the uncoated substrate (S), AC-PEO-coated specimens (A, B and C) and hard anodized sample (HA) in the 3.5 wt% NaCl corrosive medium was assessed by polarizing the samples over a potential range of − 500 mV to 3000 mV, and the corresponding data are presented in Fig. 8. The potentiodynamic polarization test parameters, i.e. exchange current density (i_{corr}) and corrosion potential (E_{corr}), are used to understand the samples' corrosion characteristics through Tafel analysis in the linear region (i.e. ± 250 mV) around OCP, and are represented in Table 7. The E_{corr} describes the sample's thermodynamic tendency for corrosion, and i_{corr} describes the corrosion kinetics. The relatively higher thermodynamic stability of the sample against the corrosion reaction can be evident from the higher E_{corr} value, whereas lower i_{corr} value indicates the sluggish corrosion reaction. The corrosion potential and exchange current density values of the coatings along with substrate are presented in Table 7. Among the coated samples, sample B exhibits the least affinity to involve in the electrochemical interactions. The i_{corr} values of A, B, C and HA coatings are $8.50(\pm 0.18) \times 10^{-4}$ mA/cm^2, $5.63(\pm 0.28) \times 10^{-6}$ mA/cm^2, $3.46(\pm 0.11) \times 10^{-4}$ mA/cm^2 and $2.70(\pm 0.16) \times 10^{-5}$ mA/cm^2, respectively. In comparison with the uncoated substrate ($i_{corr} = 1.33(\pm 0.14) \times 10^{-3}$ mA/cm^2), all the oxide coatings reveal superior corrosion resistance. Among all coatings, AC-PEO sample B shows good corrosion resistance. PEO coatings mainly consist of two different layers, a compact inner layer and an outer porous layer. The outer layer contains micropores, while the inner layer is more compact than the HA coating. In HA coating, micropores are continuous or go over the coating. The plasma discharge melting product will cap most of the discharge defects composed in the PEO process's initial state due to continuous passive film breakdown, molten metal solidification and reconstruction. The PEO-treated sample B shows superior corrosion resistance among all coatings under investigation owing to its higher inner barrier layer thickness. PEO coatings A and C are preferable in real time, despite their relatively lower corrosion resistance compared to the HA sample, owing to their better scratch resistance as discussed in the previous session.

4 Conclusions

In summary, the effect of variation in the electrolyte concentration on the thickness, surface morphology, scratch, and corrosion resistance of the AC-PEO coatings compared with hard anodized coatings on the AA7075-T6 condition was studied. The XRD patterns of all AC-PEO specimens

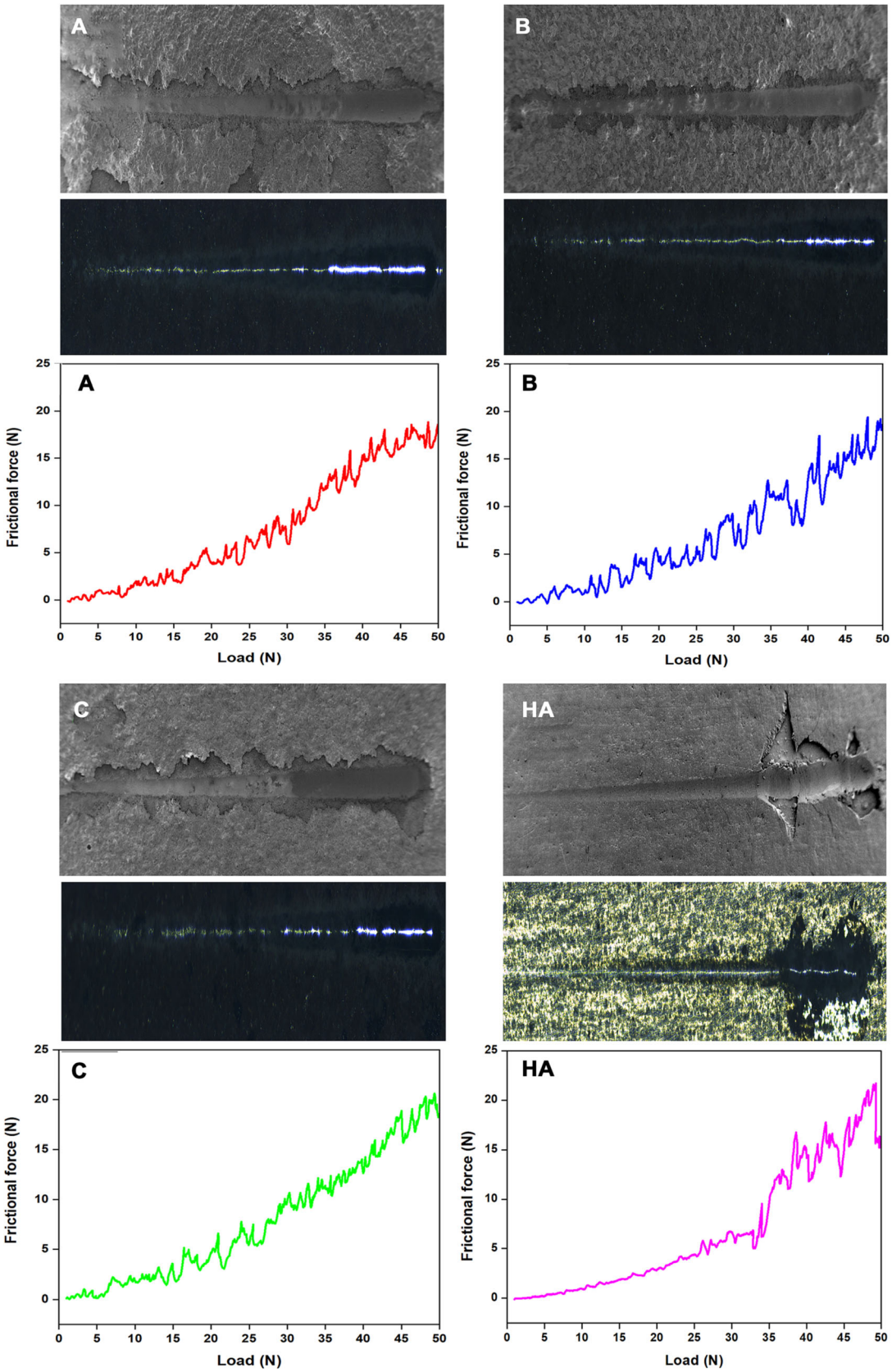

Fig. 7 FESEM, panoramic optical micrographs and the corresponding friction force versus load curves of the PEO-treated samples A, B, C and HA sample

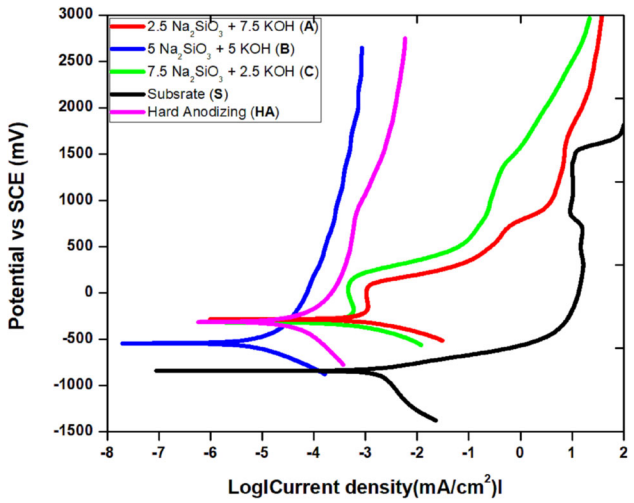

Fig. 8 Potentiodynamic polarization curves of the substrate (S), PEO-treated samples A, B, C and HA sample in 3.5 wt% NaCl solution

Table 6 Critical load (L_c) and frictional force (F_t) of the AC-PEO-treated samples (A, B and C) and hard anodizing (HA) sample

Sample code	L_C (N)	F_t (N)
A	33.5(± 2.2)	9.4(± 0.6)
B	41.5(± 1.8)	13.1(± 1.1)
C	37(± 1.5)	11.8(± 0.8)
HA	28(± 0.7)	5.7(± 0.4)

Table 7 Potentiodynamic polarization parameters of the substrate (S), PEO-treated samples A, B, C and HA sample in 3.5 wt% NaCl solution

Sample code	E_{corr} (mV)	i_{corr} (mA/cm^2)
S	− 841.45(± 12)	1.33(± 0.14) × 10^{-3}
A	− 284.61(± 14)	8.50(± 0.18) × 10^{-4}
B	− 542.48(± 20)	5.63(± 0.28) × 10^{-6}
C	− 317.99(± 15)	3.46(± 0.11) × 10^{-4}
HA	− 312.13(± 10)	2.70(± 0.16) × 10^{-5}

are mainly comprised of γ-Al_2O_3 phase. All AC-PEO coatings exhibited higher scratch resistance than HA coatings. Among all the AC-PEO coatings, specimen B with equal concentration (5 g/l Na_2SiO_3 + 5 g/l KOH) showed high corrosion resistance (i_{corr} = 5.63(± 0.28) × 10^{-6} mA/cm^2) and good scratch resistance (L_c = 41.5 (± 1.8) N) than the uncoated substrate, A, C and HA due to dense inner barrier layer and high coating thickness. From the above results, it is concluded that the composition of electrolyte played a crucial part in ascertaining coating characteristics. The equi-concentrated electrolyte of Na_2SiO_3 (5 g/l) and KOH (5 g/l) can be contemplated as the most favourable electrolyte system for obtaining better corrosion-resistant and scratch-resistant coatings on AA 70705 alloy using AC-PEO technique.

Acknowledgements The author (NRB) would also like to thank and acknowledge the financial support received from the Defence Research and Development Organisation (DRDO), New Delhi (No. EMR/2016/003259 dated 22-03-2017) to carry out this research

References

[1] Heinz A, Haszler A, Keidel C, Moldenhauer S, Benedictus R, and Miller W S, Mater Sci Eng A 280 (2000) 102.
[2] Eswara Prasad E, and Wanhill R J H, *Aerospace Materials and Material Technologies Vol 1: Aerospace Materials, IIM Series*, Springer Singapore (2017).
[3] Yu M, Dong H, and Shi H, Appl Surf Sci 479 (2019) 105-113.
[4] Agureev L, Savushkina S, Ashmarin A, Borisov A, Apelfeld A, Anikin K, Tkachenko N, Gerasimov M, Shcherbakov A, Ignatenko V, and Bogdashkina N, Metals 8 (2018) 459.
[5] Arunnellaiappan T, Kishore Babu N, Rama Krishna L, and Rameshbabu N, Surf Coat Technol 280 (2015) 136.
[6] Wang R, Wang L, He C, Lu M, and Sun L, Surf Coat Technol 360 (2019) 369.
[7] Abdel-Gawad S A, Osman W M, and Fekry A M, Surf Interfaces 14 (2019) 314.
[8] Stergioudi F, Vogiatzis C A, Gkrekos K, Michailidis N, and Skolianos S M, Corros Sci 91 (2015) 151.
[9] Thiemea M, Strellera F, Simonb F, Frenzelb R, and White A J, Appl Surf Sci 283 (2013) 1041.
[10] Gonzalez E, Vejar N, Solis R, Muñoz L, Victoria Encinas M, and Paez M, *Sol–Gel Method- Design and Synthesis of New Materials with Interesting Physical, Chemical and Biological Properties*, (ed) Aguilar G V, Intech open, London (2019) p 75.
[11] Lawal J, Kiryukhantsev-Korneev P, Matthews A, and Leyland A, Surf Coat Technol 310 (2017) 59.
[12] Assadi H, Kreye H, Gärtner F, and Klassen T, Acta Mater 116 (2016) 382.
[13] Tesar T, Musalek R, Medricky J, Kotlana J, Lukac F, Pala Z, Ctibor P, Chraska T, Houdkova S, Rimal V, and Curry N, Surf Coat Technol 325 (2017) 277.
[14] Gökhan Demira A, and Alberto Biffi C, J Manuf Process 37 (2019) 362.
[15] Arunnellaiappan T, Ashfaq M, Rama Krishna L, and Rameshbabu N, Ceram Int 42(2016) 5897.
[16] Sreekanth D, and Rameshbabu N, Mater Lett 68 (2012).
[17] Arun S, Hariprasad S, Saikiran A, Ravisankar B, Parfenov E V, Mukaeva V R, and Rameshbabu N, Surf Coat Technol 363 (2019) 301.
[18] Sharma A, Jang Y J, and Jung J P, J Mater Eng Perform 26 (2017) 5032.
[19] Mohitfar S H, Mahdavi S, Etminanfar M R, and Khalil-Allafi J, J Alloys Compd 842 (2020) 155988.
[20] Lerner L M, Trans Inst Met Finish 88 (2010).
[21] Hariprasad S, Gowtham S, Arun S, Ashok M, and Rameshbabu N, J Alloys Compd 722 (2017) 698.
[22] Sieber M, Mehner T, Dietrich D, Alisch G, Nickel D, Meyer D, Scharf I, and Lampke T, Surf Coat Technol 240 (2014) 96.
[23] Walsh F C, Low C T J, Wood R J K, Stevens K T, Archer J, Poeton A R, and Ryder A, Trans Inst Met Finish 87 (2009) 122.
[24] Hussein R O, and Northwood D O, in *Developments in Corrosion Protection*, (ed) Aliofkhazraei M, Intech open, Croatia (2014) p 201.

[25] Mohedano M, Lu X, Matykina E, Blawert C, Arrabal R, and Zheludkevich M L, *Plasma Electrolytic Oxidation (PEO) of Metals and Alloys* (2018), p 423.
[26] Saikiran A, Hariprasad S, Manojkumar P, Rama Krishna L, and Rameshbabu N, Surf Coat Technol 394 (2014) 125888.
[27] Manojkumar P, Lokeshkumar E, Saikiran A, Govardhanan B, Ashok M, and Rameshbabu N, J Alloys Compd 825 (2020) 154092.
[28] Yang Z, Wu Y K, Zhang X Z, Wang D D, Liu X T, Wu G R, Li D L, Yu S X, and Shen D J, Surf Interfaces 16 (2019) 199.
[29] Babaei K, Fattah-alhosseini A, and Molaei M, Surf Interfaces 21 (2020) 100677.
[30] Hariprasad S, Saikiran A, Premchand C, Rama Krishna L, and Rameshbabu N, J Magnes Alloy (2020, in press).
[31] Li Q, Liang J, Wang Q, in *Modern Surface Engineering Treatments*, (ed) Aliofkhazraei M, Intech open, Croatia (2013), p 75.
[32] Santosh Prasad S, Etsushi T, Yoshitaka A, and Hiroki H, Corros Sci 55 (2012) 90.
[33] Pillai A M, Rajendra A, and Sharma A K, J Appl Electrochem 48 (2018) 543.
[34] Khan R H U, Yerokhin A, Li X, Dong H, and Matthews A, Surf Coat Technol 205 (2010) 1679.
[35] Jiang B L, and Wang Y M, in *Surface Engineering of Light Alloys: Aluminium, Magnesium and Titanium Alloys*, (ed) Dong H, Woodhead Publishing (2010) p 110.
[36] Yerokhin A L, Shatrov A, Samsonov V, Shashkov P, Pilkington A, Leyland A, and Matthews A, Surf Coat Technol 199 (2005) 150.
[37] Ghafaripoor M, Raeissia K, Santamaria M, and Hakimizad A, Surf Coat Technol 349 (2018) 470.
[38] Kwolek P, Krupa K, Obłoj A, Kocurek P, Wierzbinska M, and Sieniawski J, J Mater Eng Perform 27 (2018) 3268.
[39] Rama Krishna L, Sudha Purnima A, and Sundararajan G, Wear 261 (2006) 1095.
[40] Alexandre Becerik D, Ayday A, Cenk Kumruoglu L, Can Kurnaz S, and Ozel A, J Mater Eng Perform 21 (2012) 1426.
[41] Fattah-Alhosseini A, Vakili-Azghandi M, and Keshavarz M K, Acta Metall Sin (Engl Lett) 29 (2016) 274.
[42] Yerokhin A L, Snizhko L O, Gurevina N L, Leyland A, Pilkington A, and Matthews A, J Phys D Appl Phys 36 (2003) 2110.
[43] Ikonopisov S, Girginov A, and Machkova M, Acta 24 (1979) 451.
[44] Rama Krishna L, Rybalko A V, and Sundararajan G, Process for forming coatings on metallic bodies and an apparatus for carrying out the process, (2005) US 6,893,551 B2.
[45] Snizhko L O, Yerokhin A L, Pilkington A, Gurevina N L, Misnyankin D O, Leyland A, and Matthews A, Electrochim Acta 49 (2004) 2085.
[46] Saikiran A, Hariprasad S, Arun S, Rama Krishna L, and Rameshbabu N, Surf Coat Technol 372 (2019) 239.
[47] Wheeler J M, Curran J A, and Shrestha S, Surf Coat Technol 207 (2012) 480.
[48] Ramakrishnan E, Premchand C, Manojkumar P, and Rameshbabu N, Mater. Today (2021, in press).